# Improving Accuracy of Precessing Binary Black Hole Waveform Templates Using Gaussian Process Regression

Emily Phillips Longley, Advisors: Dr. Siong Heng, Dr. Chris Messenger

*Institute for Gravitational Research, University of Glasgow, Scotland, UK., Department of Physics, University of Florida, Gainesville, FL 32611-8440 USA. , Department of Physics, Carleton College, Northfield, MN, 55057, U.S.A.*

August 11, 2015

**Abstract**

With the first data run for advanced LIGO (aLIGO) in Fall 2015 we are quickly approaching a regime in which detection of gravitational waves is highly plausible . Not only do the advanced detectors represent the most promising experimental verification of Einstein's theory of general relativity, but they additionally usher in the next era of astronomy, bringing in a new way of exploring our universe and complimenting existing astronomical observations. These observations have the potential to transform our understanding of astrophysical objects, but only if the source parameters can be accurately estimated. Such parameter estimation is currently dependent on the usage of waveform templates. Accurate templates can be computed using numerical methods, but the prohibitive cost of these simulations means this can only be done for a small handful of parameters. Inference will therefore be reliant on approximate, analytical waveforms. In [**?**] a novel method to fold model uncertainties into data analysis is proposed; the waveform uncertainty is analytically marginalized over using a prior distribution constructed by using Gaussian process regression to interpolate the waveform difference from a small training set of accurate templates. We present the first steps to applying this method using the latest binary black hole (BBH) Numerical Relativity (NR) catalog produced by the GAtech NR group, and analytic waveforms from the model PhenomP in the LAL database. In addition, we present the results of using Gaussian process regression to produce error estimates in the catalog's seven dimensional parameter space with the aim that such information can guide the NR community to regions of parameter space where new simulations are most needed.

## 1 INTRODUCTION

According to Einstein's theory of General Relativity astrophysical events involving extremely massive objects cause perturbations in space-time that propagate as waves. These perturbations are detectable on Earth with the usage of interferometers - optical instruments that use isolated test masses to detect minute oscillations when ripples of the waves cause the surrounding spacetime to bend. Gravity is a weak force, making gravitational waves very weak and difficult to detect. In addition, just as waves in water decrease in strength as they move away from the source, gravitational waves are weaker once they reach us, then when they began. For example, the calculated effect of gravitational waves on earth from sources including spiraling black holes and neutron stars yields a stretching and compressing of space by only about one part in one trillion billion. []

Advanced LIGO will begin operation in Fall 2015. The detector is composed of two interferometers with 4km arms and one with 2km arms [**?**] with mirrors attached to vibration-isolated test masses at the end of each arm. Lasers make continuous measurements of the distance between each of the test masses. The masses are free to move so that when a gravitational wave passes, the distance between the masses will fluctuate. The greater the distance between the masses the more sensitive the lasers are to small fluctuations. The detector is expected to make the first direct observations of gravitational waves when it reaches design sensitivity.

These observations, combined with advances in pulsar timing arrays and space-based interferometers, have the potential to allow for true gravitational wave-based astronomy. This goal however, can only be achieved if source parameters, e.g., the mass, and spin, can be accurately estimated. Data analysts must be able to discriminate a signal of astrophysical origin from instrumental artifacts in the interferometer data and to extract values for the full range of parameter space for the signal progenitor. This characterization of the signal relies on matching it with a waveform template. This can be done in several ways. One way is through a detection pipeline for the signal, and will likely provide the first indication of detection. This relies on parameter estimation through the association with a template corresponding to the largest signal-to-noise ratio (SNR). Another technique used is Bayesian Inference, which is the approach taken with this project, and is discussed in section 4. All current data analysis techniques rely on waveform templates and accurate detection and interpretation of the signal requires model waveforms that capture the phenomenology of all likely astrophysical configurations of the progenitor.

There are two ways of generating such waveforms. One is approximate, based on phenomenological analytical equations which are computationally quick and cheap. The other is exact, based on numerical relatively, and is very computationally

expensive and difficult to generate. We present the first attempt to match the two types of waveforms, with the aim of improving the accuracy of the approximate waveform template with information gathered from the exact waveform. Additionally, we provide information about the most uncertain regions in the seven-dimensional parameter space of the latest waveform catalogue provided by the NR group at GAtech, in the hopes that this provides insight into the most efficient use of spending computational time in the generation of new waveforms.

# 2 BINARY BLACK HOLE MERGERS

One of the most promising sources for the Advanced detectors, with a realistic expected rate of 20 such events per year observed at design sensitivity (AASi et al. 2013b) [**?**], are binary black hole (BBH) mergers. Because of their density, black holes in merger events produce extremely intense gravitational radiation, with numerical simulations of the evolution of a black hole coalescence suggesting that an estimated 5% of the total initial mass of the system is radiated away as gravitational energy [**?**] This process can be broken down into three major stages; inspiral, merger and rindown. As the two black holes orbit one another, there is a massive loss of energy and the separation between the two black holes decreases, and they spiral closer together. This causes the frequency at which they orbit and the amplitude of the gravitational radiatiaon emitted to increase, causing the system to lose more energy and the inspiral to speed up [**?**]. Eventually the two black holes collide and coalesce with one another to form one larger, spinning black hole known as a Kerr black hole. Immediately after formation, this will give off gravitational waves with rapidly decreasing amplitude - the ringdown stage. An example of a simulated waveform from the merger of a black hole binary system showing these features is shown in figure 1.

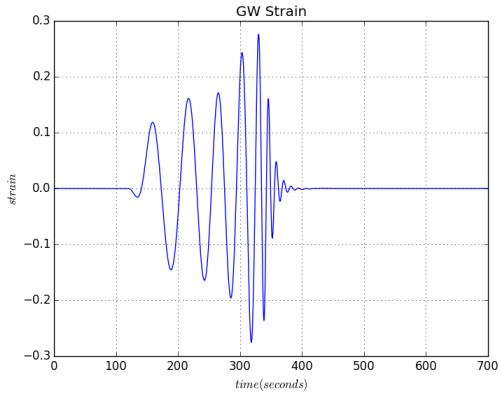


Figure 1: An example numerical relativity waveform model of a binary black hole merger event, for a system with a total mass of 200 $M_{\odot}$ showing the inspiral, peak at coalescence, t = 320s, and the subsequent ringdown of the resulting black hole.

The construction of a model of the GW signal from generic configurations of spinning-black-hole binaries, through inspiral, merger and ringdown, is one of the most pressing theoretical problems being tackled by today's GW data astronomers. [**?**]. BBH's provide a wealth of interesting behavior and ALIGO will be sensitive to merging BBH systems out to several Gpc. The majority of galaxies, including our own, have massive black holes at their centers. Given the age of the Universe, most of the larger galaxies we see today are the result of two or more galaxy collisions. Thus, it is very probable that the two black holes from previously separate galaxies would be in a binary orbit around each other at the center of the new, larger galaxy. Examining the movements of these extremely large masses allows for the mapping out of the curvature of spacetime in those areas. Quantitative knowledge of the strain caused by the two black holes will yield information about the shape and behavior of the event horizon of a black hole and how black holes affect galactic evolution.[] However, because of the complexity of this process, primarily that of the precession effects caused by the black-hole spins, these systems are a challenge to model accurately. The waveforms that we work with in this project represent two different approaches to modeling this complicated astrophysics.

# 3 DATA SETS

Currently, the field of numerical relativity is very active in tackling the challenge of simulating these complex systems. All essential elements of the gravitational strain produced by a given BBH system is captured numerically in a multi-dimensional parameter space. The binary's early inspiral can be modeled with analytic post-Newtonian (PN) calculations, but the late inspiral and merger require 3D numerical solutions of the full nonlinear Einstein equations. These expensive numerical relativity (NR) calculations must span a parameter space of binary configurations that covers, for noneccentric inspiral, seven dimensions: the mass ratio of the binary, and the components of each black hole's spin vector; the total mass of the system is an overall scale factor. [**?**] (see appendix for a more detailed explanation of these parameters).

For our work, we used the newly released, gravitational-wave strain for GATech BBH Numerical Relativity simulations. There are a total of 421 distinct NR simulations, presented in the time domain, in the catalogue for nine different series, (a complete list of the series is also found in the appendix). In figure 2, we show a sample NR waveform from the catalog.

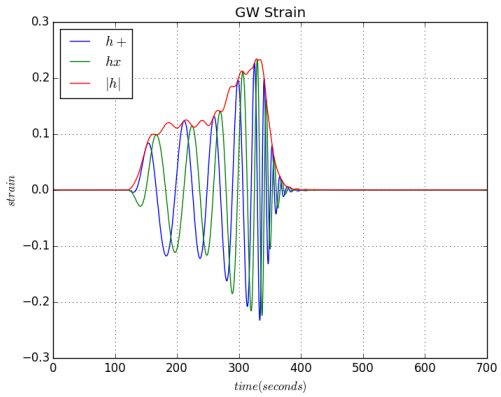


Figure 2: A sample waveform from the BBH catalogue, scaled to a total mass of with a total mass of 200 $M_{\odot}$

However, a mapping done by [**?**] with at least four simulations in each direction of parameter space (which is sufficient to cover the same parameter space as analytical waveforms) implies that modelling these systems requires $4^7$ $O(10^4)$ numerical simulations. Thus NR waveforms alone cannot be used for inference of LIGO data. Instead, because of their accuracy, numerical relativity waveforms are primarily used to mimic real signals, to be used in the development and testing of gravitational wave data analysis techniques. Instead inference is reliant on approximate, analytical waveforms.

## 3.1 PHENOMOLOGICAL APPROXIMATE WAVEFORMS

The current and first of its kind, approximate model for the GW signal due to spinning BBH's is "PhenomP" available in the LAL data base in the frequency domain. It captures all the basic phenomenology of the seven-dimensional parameter space of binary configurations with only three key parameters. The initial inspiral is modeled analytically with PN calculations. The late inspiral, merger and ringdown stages of the waveforms are defined by an underlying non-precessing-binary model by the binary's mass ratio and an effective total spin parallel to the orbital angular momentum, determining the inspiral rate. The non-precessing binary waveforms are then "twisted up" with approximate expressions for the processional motion. Although many GW models, such as EOBNR [8] Moore and Gair or IMRPhenomC are constructed by using NR simulations to fit the values of free parameters in extended analytical models, IMRPhenomP is constructed via a transformation of a non-precessing model PhenomC and did not use any precessing-binary numerical simulations in its construction. This is the first frequency-domain inspiral-merger-ringdown model of generic binaries. Frequency domain models are essential for both efficient GW searches and parameter estimation. The model uses the highest-order (closed-form) PN expressions available. [**?**] In figure 3, we have a sample PhenomP waveform presented in the frequency domain.

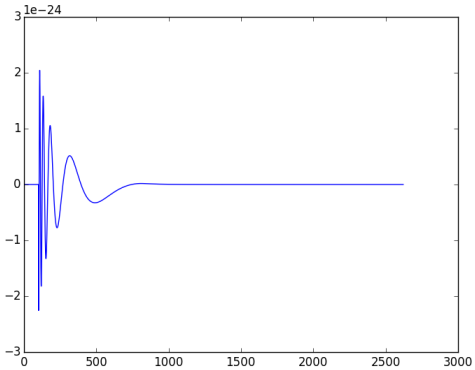


Figure 3: A sample analytical approximate solution, presented in the frequency domain, to a precessing BBH system with q = 2.00.

## 3.2 MATCHING THE WAVEFORMS

In order to begin interpolating the waveform differences between the NR and approximate waveforms, the two data sets must be matched. That is, in order for GPR to return accurate results, the only distinguishing feature between the two

waveforms must be that one is an NR and one is an analytical model for the same representation of the same BBH system. Each of the NR waveforms was scaled by a specific mass for each waveform that corresponds to a reference frequency of 10Hz. The waveform was then smoothed and resampled at a sampling rate of (This was adapted to scale the waveform so that every waveform was at a 200 solar mass. For the approximate waveform, a reference frequency of 10Hz was inputted, a q value for the the waveform and a S_x, S_y and S_z spin for each of the black holes. For these parameters, it was a simple matter of changing the NR parameters from polar coordinates to cartesian coordinates. Theta represents the polar angle between the spin and the oribital angular momentum L at t=0 for the NR run. a is the dimensionless spin magnitude, also at the beginning of the ru, corresponding to the spin vector that has an angle of theta. At t=0, the orbital angular momentum L is pointing in the +Z axis, so theta is measured from the z-axis so I inputed Sz = a*cos(theta) adn Sy = a*sin(theta), Sx = 0. Each of the waveforms must be scaled to a given total mass for the system. We scaled both sets to a mass of 200 $M_{\odot}$ as this represents the highest amplitude strain that remains in the aLIGO frequency band [**?**]. The NR waveforms were then converted to the frequency domain via a fast-fourier-transform (fft). All of the waveforms in the RO3 series of the catalog is shown in figure 4, represented by the instantanous frequency as a function of time.

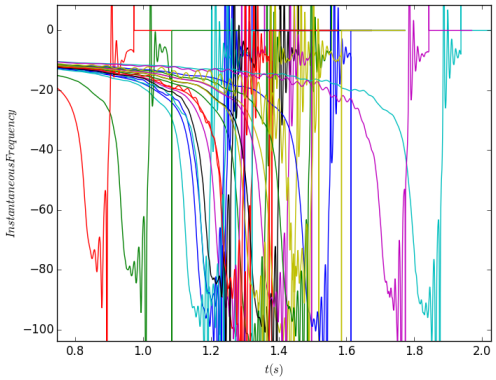


Figure 4: All of the waveforms in the RO3 series shown here in the frequency domain.

The two waveforms were then compared given the values for the set of parameters shown in figure 5. Figures 5 and 6 show the overlap of the NR and approximate waveform by phase and strain.

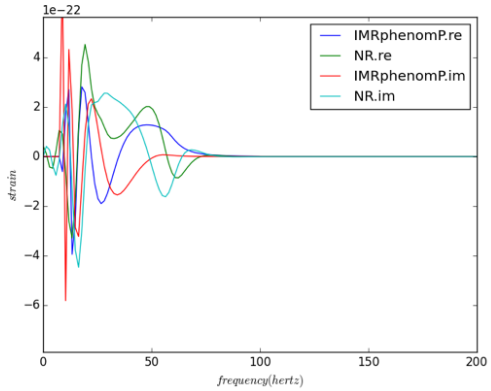


Figure 5: The unwrapped phase of the two waveforms as a function of time.

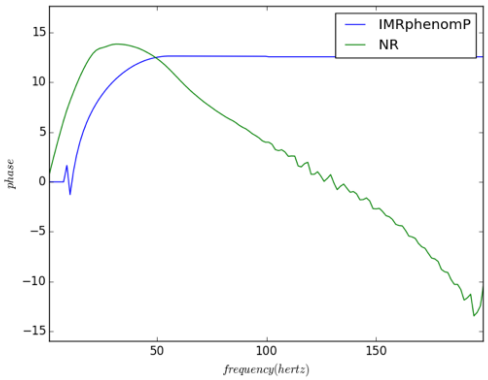


Figure 6: The overlapping

The PhenomP waveforms are composed of the l=2 and m=—2— modes, while the NR waveforms only represents the l,m = (2,2) modes. However, in [6] the contributions to the emitted waves of each of the spherical harmonic modes are investigated and it is shown that the l = 2 m 2 modes are by far the most dominants, thus, for our purposes this overlap is sufficient for accurate GPR interpolation. Our current overlap of the waveforms shows that the amplitudes are now within a factor of a few. The next step to matching the waveforms is to make a time and phase shift with PhenomP so that it matches the NR waveforms. These represent steps taken since the very recent release of the BBH catalog. Because the PhenomP waveforms were created solely in the frequency domain, there is no strict reference time at which the waveform begins. Thus, the next step to matching the two sets of waveforms, is to create an algorithm that maximizes the match of the waveforms with a function of a time and phase shift.

# 4 MODIFIED LIKELIHOOD

As was discussed, due to the computational expensive of NR waveforms, GW inference will rely on approximate analytical waveforms. These approximations introduce systematic errors in the model that are have been shown to be potentially significant for both ground [7] and space-based detectors [1]. Ours is a Bayesian approach, however these systematic errors are present in any data analysis technique when using approximate waveforms. Bayesian inference is based upon Bayes' theorem which relates the current probability to prior probability. The prior, is the initial distribution of the parameters before any data is observed and the posterior distribution is the distribution of the parameters after taking into account the observed data. Bayes' theorem states that the posterior is proportional to the prior times the likelihood,

$$\begin{aligned} Pr(D|\lambda, I)XPr(\lambda|I) &= Pr(D|I) * Pr(\lambda|D, I) \\ LikelihoodxPrior &= Evidence * Posterior \\ L(\lambda) * \pi(\lambda)d\theta &= X * p(\lambda)d\lambda \end{aligned} \tag{1}$$

where the likelihood of a set of parameter values, given a set of outcomes, is equal to the probability of those observed outcomes given those parameter values. In a Bayesian detection, the most important value to evaluate is the likelihood. When using approximate waveform templates we are limited to an approximate evaluation for the likelihood. There are two related problems with using approximate likelihood regarding both detection and parameter estimation. If the model is a poor representation of any signal present then the integral of the posterior over parameter space (the evidence, a way to select which model is most probable) will be underestimated. This decreases the probability that the signal will be detected and potentially increases the chance of incorrect model selection. This causes inaccurate detection. Inaccurate parameter estimation occurs when the position of the peak of the posterior evaluated using an approximate model is shifted relative to the true position. This has been shown to occur by more than the statistical error due to random noise [7]. This shift is demonstrated in figure 7.

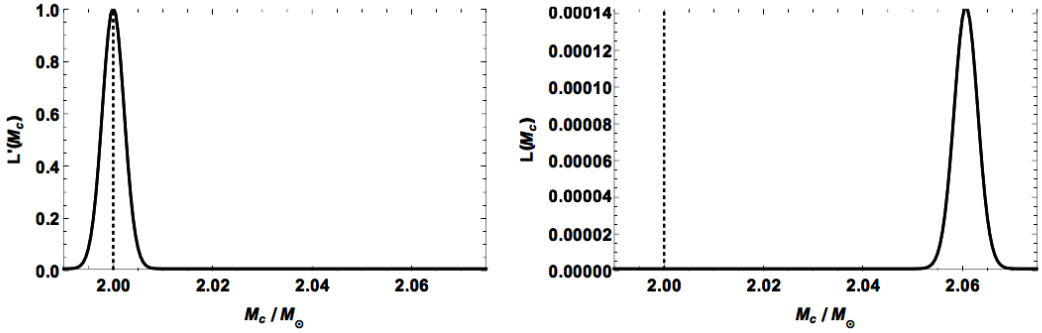


Figure 7: The results of Bayesian analysis using an approximate (3.5 PN IMR PhenomC) waveform. The exact value is shown with the dotted line. The exact likelihood is peaked at the true value with value 1 at that point. The approximate likelihood shows a suppressed and shifted peak.

In [**?**] a new method to fold model uncertainties into data analysis is proposed; the waveform uncertainty is analytically marginalized over using a prior distribution constructed by using Gaussian process regression to interpolate the waveform difference from a small training set of accurate (BBH NR catalog) templates and the approximate (PhenomP) templates. The following is a summary of their proposed method applied to our data sets. The NR BBH catalog is fully characterized by a set of seven parameters $\vec{\lambda}$. We then have the ability to calculate the accurate waveform template h($\vec{\lambda}$ for each of the 422 waveforms contained in the catalogue. Additionally we can compute the approximate, H($\vec{\lambda}$ at the same points in parameter space. We can then relate the templates by their waveform difference:

$$H(\lambda) = h(\lambda) + \delta h(\lambda) \tag{2}$$

To perform parameter estimation we must calculate the posterior distribution, $p(\vec{\lambda}|s)$, from the observed data $s$. From Bayes theorem (equation one), this is proportional to the product of the likelihood and the prior. For a detector with stationary, Gaussian noise with power spectral density Sn(f), the true likelihood is:

$$L'(s|\vec{\lambda})\alpha exp(-\frac{1}{2}\langle s - h(\vec{\lambda})|s - h(\vec{\lambda})\langle) \tag{3}$$

With the inner product as defined in [**?**]. Because of the computational expense of NR waveforms it is impossible to sample from this distribution and we must instead use the PN waveforms to calculate an approximate likelihood.

$$L(s|\vec{\lambda})\alpha exp(-\frac{1}{2}\langle s - H(\vec{\lambda})|s - H(\vec{\lambda})\rangle) \approx L' \tag{4}$$

The proposed modified likelihood accounts for the uncertainty in the PN waveforms:

$$\mathcal{L}(\vec{\lambda})\alpha \frac{1}{\sqrt{1+\sigma^2(\vec{\lambda}}} x exp(-\frac{1}{2}\frac{< s - H(\vec{\lambda} + \mu(\vec{\lambda})|s - H(\vec{\lambda} + \mu(\vec{\lambda}) >}{1+\sigma^2(\vec{\lambda}}) \tag{5}$$

Where the best-fit waveform has shifted by $\mu(\vec{\lambda})$, the best estimate of the waveform difference returned by GPR (the exact process of GPR is discussed in section 3). The $\frac{1}{\sqrt{1+\sigma^2(\vec{\lambda}}}$ term broadens the likelihood distribution, accounting for the error accumulated in the interpolation between the waveform differences. The prior on the waveform difference thus includes the information available from the limited number of available NR waveforms. The new likelihood takes no appreciable extra time to evaluate compared to the likelihood in equation five because the most expensive step is evaluating the inner product which is common to both. One defect in the above analysis is that the GPR assigns a single error value to the interpolated waveform. This is overly conservative as the waveform models have strongly frequency dependent errors. This can be accounted for by generalizing the above analysis by modeling the waveform error in each frequency bin as an independent Gaussian process. In can be accomplished by adding a frequency dependence to the likelihood, however, as our analysis is done in the frequency domain, each bin is could be naturally treated as its own gaussian process with a noise component on each observed value as in figure 8.

In [**?**] this approach was applied to a toy problem, using non-spinning PN waveforms to the extraction of the chirp mass of a high order PN waveform using a lower order PN wave- form. In place of the NR waveforms 3.5 PN order waveform were used, while the approximate waveform was a 3PN waveform. The waveforms were dependent on one parameter, $\lambda$ = chirp mass. In our work we extend their proposal by using real NR waveforms, (the GAtech BBH catalog) and approximate PN waveforms (PhenomP) while interpolating over the seven parameters that characterize the NR waveforms (see appendix).

# 5 DATA ANALYSIS

## 5.1 SUMMARY OF GAUSSIAN PROCESS REGRESSION

GPR is a method of interpolation for which the interpolated values are modeled by a Gaussian process governed by a prior covariance. This is in contrast to most regression techniques in which a piecewise polynomial function is chosen to optimize smoothness of fitted values. GPR is the ideal interpolator because the prediction is probabilistic, allowing one to compute empirical confidence intervals and exceedance probabilities, so that not only is a waveform difference predicted at a certain point in parameter space but the associated error with this prediction is returned as well. Additionally, GPR is versatile and non-parametric different linear regression models and correlation models can be specified, allowing us to incorporate prior beliefs about the accuracy of the templates in a non-parametric manner, and perform the marginalization analytically. Figure 8 illustrates a simple GPR fit to a function given 6 observations (exact values for the function).

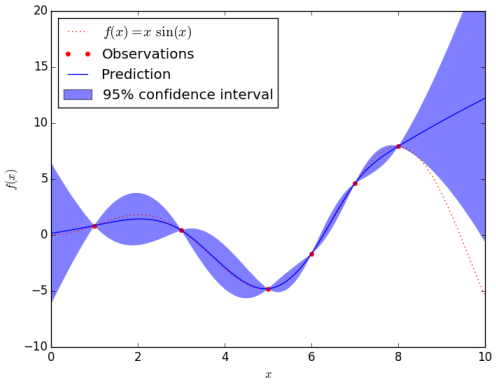


Figure 8: A simple one-dimensional regression exercise computed for the noise-free case with a cubic correlation model (scikit-learn).

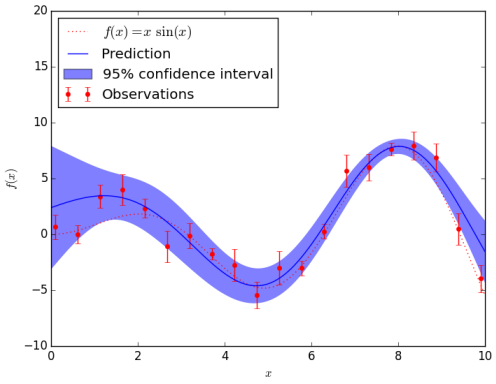


Figure 9: A simple one-dimensional regression exercise computed for the noisy case with a squared Euclidean correlation model. (scikit learn)

With this method, the model parameters are estimated using the maximum likelihood principle. The two figures illustrate the both the interpolative power of GPR, as well as its ability to simultaneously compute the error of the interpolation, depicted here by the pointwise 95% confidence interval.

## 5.2 Reconstruction of Approximate Waveforms

Suppose we have access to exact waveforms at a few values of the parameters and can cheaply compute approximate waveforms at the same parameter values. Our train set is thus the waveform differences,

$$\mathcal{D} = (\vec{\lambda}_i, \delta h(\vec{\lambda}))|i = 1, 2, ...n) \tag{6}$$

Because we only have a limited number of NR waveforms, our training set is limited. We therefore use GPR to interpolate between the waveforms to return a prediction for the waveform difference at the needed locations in the seven dimensional parameter space. It should be noted that our method allows for incorporating any error (however minimal) that is known to be associated with the NR waveforms, however, our method treats them as exact (as in noise-free rather

than noisy example GPR (figure 8). An example of this interpolation using two waveforms of different masses is shown in figure 10.

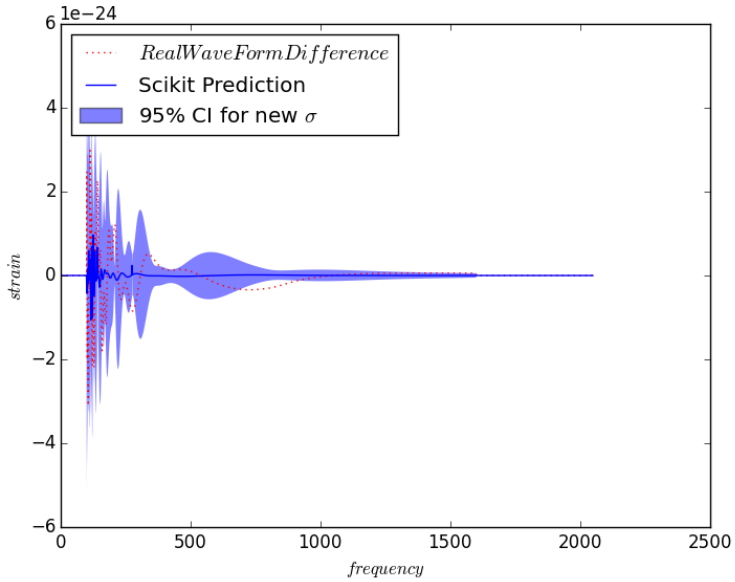


Figure 10: A sample interpolation of the waveform difference between two NR waveforms of scaled to differing masses.

Thanks to the release of the new NR catalog form GAtech, we are able to interpolate throughout the entire seven dimensional parameter space that defines a BBH system waveform. In [?] $\mathcal{D}$ consisted of the waveform difference computed at five chirp masses. Figure 11 shows the results of GPR interpolation at each of these values.

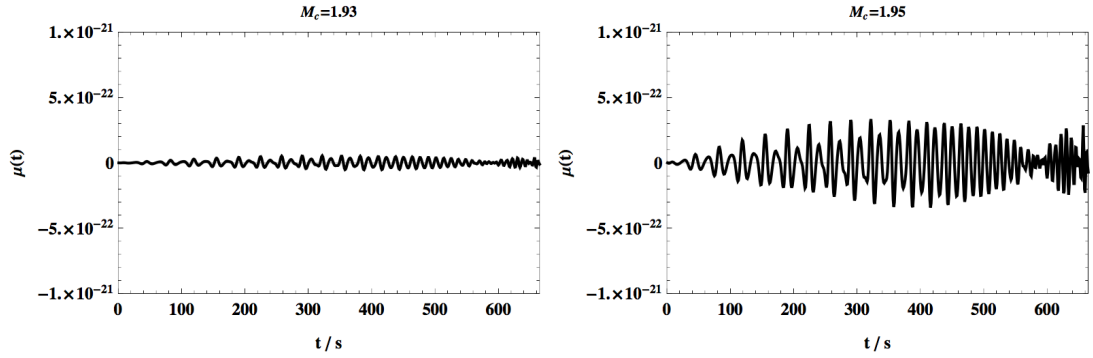


Figure 11: The results returned by GPR to interpolate the waveform difference across the range of chirp mass used in the search.

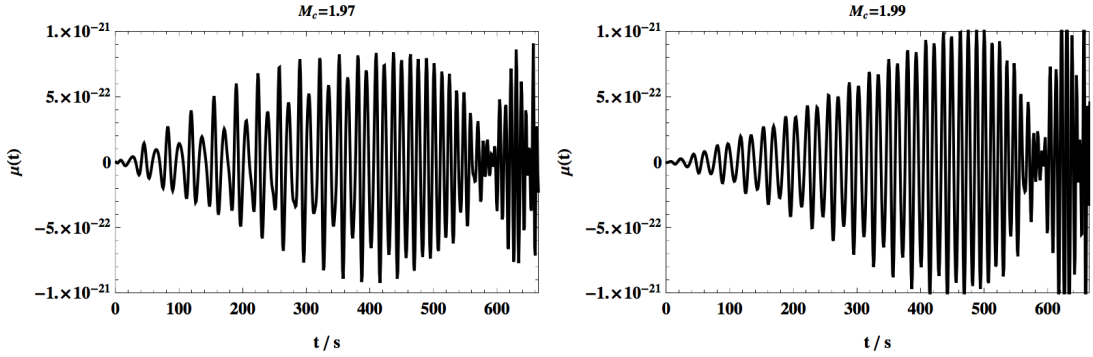


Figure 12: The results returned by GPR to interpolate the waveform difference across the range of chirp mass used in the search.

Our training set contains the exact waveform difference computed at 422 waveforms of various values for the parameters. We can thus feed GPR 422 known observations. This greatly increases the accuracy of the returned interpolated waveform differences, and allows us to explore the seven dimensional parameter space by extending the method used to search for a single parameter.

## 5.3 Error Estimates in NR Parameter Space

The advantages of GPR as an interpolator that produces a probabilistic prediction allows for one to compute empirical confidence intervals and exceedance probabilities that can be refit in some region of interest. This property is particularly useful in GW analysis in that it has the ability to return the error value for a waveform in any region of parameter space not yet fully spanned by accurate waveforms. With our BBH data set, this means that we can use GPR to interpolate to any point in the seven-dimensional parameter space and return the waveform error at that point. It additionally means that we can segregate this to any region of parameter space (or any particular series) and still return an accurate result. This information could be applied to future NR simulations, in order to determine the areas in which it would be most beneficial to generate a new waveform. The following plots were completed with the RO3 series waveforms as observations used in GPR.

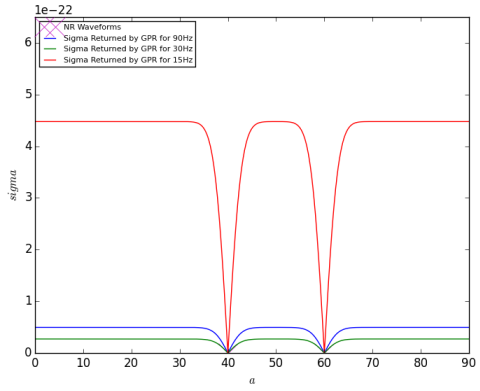


Figure 13: The GPR error estimate as a function of the dimensionless spin of the black holes, with q = 2.00, and $\theta = 60$.

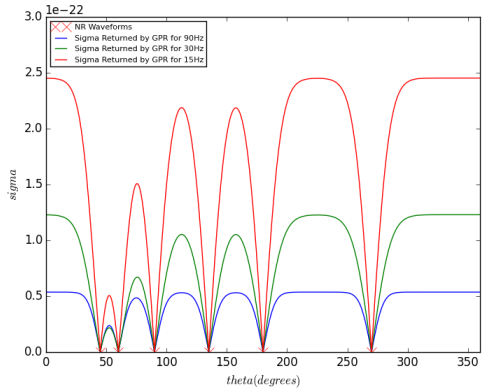


Figure 14: The GPR error estimate as a function of $\theta$, with q = 2.00 and a = 60.

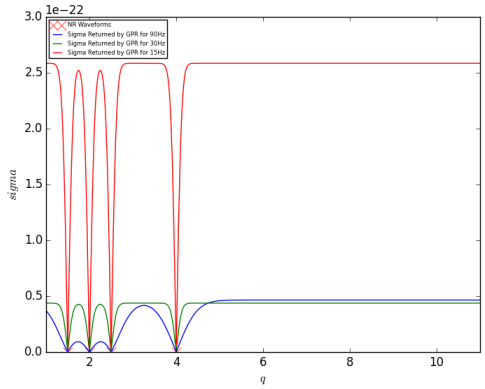


Figure 15: The GPR error estimate as a function of q, with $\theta = 45$ and a = 60.

The waveforms were scaled to a total mass of 200 $M_{\odot}$. The analysis was performed on the real part of the Fourier transformed time-domain waveforms. The GPR prediction was made for 1,000 points spanning the range of the parameter that is being examined, for example, the $\theta$ plot was produced by calculating 1,000 points between 0 and 360 (see appendix). These preliminary plots limited the parameter space to 3 dimensions: $q$, $a$ (where $a = |a1| = |a2|$) and $\theta$. In each plot, the other two parameters were kept at a constant value. The choice of frequencies correspond to "low", "medium" and "high" for a 200 $M_{\odot}$, based upon the instantaneous frequency plot 4. At parameter values represented in the RO3 waveform series, the error equals zero. The GPR error does not diverge outside of this regime, but the error tends rapidly to a finite limit of $\sigma$ , which reflects the magnitudes of the waveform differences in the set. The error is frequency dependent as expected with a lower frequency corresponding to a lower error. In this simple case, besides frequency, the error is primarily a function of the distance between the points in the 1D parameter space spanned by the interpolation.

We additionally applied the same technique to the entire catalogue, with all seven parameters. This was completed in the time domain. All waveforms were fed to GPR as observations, and the same 1,000 point resolution was spanned across the space for the $\theta$ parameter. In this case, more interesting behavior, a result of the larger parameter space, and the unevenly spaced waveforms occurs for the returned error.

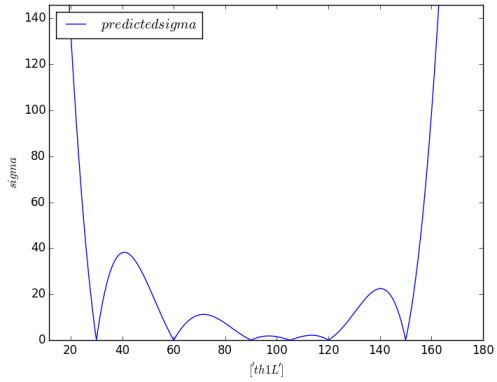


Figure 16: The GPR error estimate as a function of $\theta$, all six other parameters were held constant.

In this case, more interesting behavior, a result of the larger parameter space, and the unevenly spaced waveforms occurs for the returned error.

# 6 CONCLUSION

Following the method proposed by [**?**] we present the first steps to folding model uncertainties into gravitational wave data analysis using Gaussian Process Regression. We present the first-ever attempts to match NR BBH waveforms to analytic, using the just released GAtech catalog and the first of its kind PhenomP and usage of GPR in order to interpolate the waveform difference for usage in a modified likelihood in a higher (7) -dimensional parameter space. The next steps of this research that will be undertaken in the coming weeks is to test the accuracy of the interpolation made on the phase and time shifted waveforms by performing Bayesian analysis with the marginalized likelihood. In last part of this paper the focus has been on exploring the error returned in parameter space given a set of simulations. Although this has been applied in the field of gravitational waves research, it can be implemented in any problem where exact simulations are computationally expensive.

# Appendices

Appendix

```
q = mass-ratio m1/m2 >1
|a1| = dimensionless spin magnitude [0,1]  on BH-1
|a2| = dimensionless spin magnitude on BH-2
th1L = Polar angle between spin-1 and orbital angular momentum L at t=0 of NR run
th2L = Polar angle between spin-1 and orbital angular momentum L at t=0 of NR run
ph1 = Azimuthal angle between spin-1 and the +X-axis at t=0
ph2 = Azimuthal angle between spin-2 and the +X-asix at t=0
th12 = Angle between the two spins S1 and S2 at t=0 == acosd(S1_hat, S2_hat)
thSL = Angle beteen the total spin S=S1+S2 and orbital angular momentum L at t=0
thJL = Angle between total angular momentum J = L + S and orbital angular momentum L at t=0
```

Figure 17: A summary of the seven parameters needed to span the space of BBH waveforms.

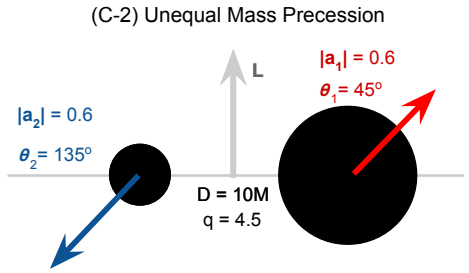


Figure 18: A diagram illustrating the physical parameters dictating the waveform created by a BBH system.

| SeriesName | TotalRuns | SeriesType |
|---|---|---|
| Eq-Series | 24 | Precession |
| Lq-series | 23 | Precession |
| Tp-series | 21 | Precession |
| Tp2-series | 20 | Precession |
| Sq-series | 63 | Precession |
| RO3-series | 22 | Precession |
| HR-series | 115 | Non-Precession |
| HRq-series | 45 | Non-Precession |
| S-series-v2 | 88 | Precession (equal-mass) |
| TOTAL RUNS | 421 | |

Figure 19: A summary of the series in GAtech's BBH

## References


[1] M. Hannam, P. Schmidt, et al. A simple model of complete precessing black-hole-binary gravitational waveforms. *Phys. Rev. Lett.* arXiv:1308.3271v2 [gr-qc] 19 Sep 2014.

[2] C. Moore, J. Gair, Novel method for incorporating model uncertainties into gravitational wave parameter estimates *Phys. Rev. Lett.* arXiv:1412.3657v1 [gr-qc] 11 Dec 2014.

[3] X. L. Fan, C. Messenger, I. S. Heng, A Bayesian approach to multi-messenger astronomy: identification of gravitational-wave host galaxies. *Astrophysical Journal* arXiv:1406:1544[astro-ph.HE] 5 Jun 2014.

[4] M. Hannam. Status of black-hole-binary simulations for gravitational-wave detection. *Classical and Quantum Gravity*, 26(11):114001, 2009.

[5] S. Fischetti, J. Healy, L. Cadonati, et al. Exploring the use of numerical relativity waveforms in burst analysis of precessing black hole mergers. *Phys. Rev. D.* 83:044019, Feb 2011.

[6] F. Pretorius. Evolution of binary black-hole spacetimes. *Phys. Rev. Lett.*, 95:121101, Sep 2005.

[7] J R Smith for the LIGO Scientific Collaboration. The path to the enhanced and advanced ligo gravitational-wave detectors. *Classical and Quantum Gravity*, 26(11):114013, 2009.